Effect of zinc oxide film morphologies on the formation of Shewanella putrefaciens biofilm

Dai, Yue; Sun, Tong; Zhang, Zhibing; Zhang, Zhenyu; Li, Jian-rong

DOI:
10.1116/1.4976003

Document Version
Peer reviewed version

Effect of zinc oxide film morphologies on the formation of Shewanella putrefaciens biofilm

Yue DaiTong SunZhibing Zhang and Zhenyu J. ZhangJian-rong Li

Citation: Biointerphases **12**, 011002 (2017); doi: 10.1116/1.4976003
View online: http://dx.doi.org/10.1116/1.4976003
View Table of Contents: http://avs.scitation.org/toc/bip/12/1
Published by the American Vacuum Society

Effect of zinc oxide film morphologies on the formation of *Shewanella putrefaciens* biofilm

Yue Dai
College of Food Science and Project Engineering, Bohai University, Food Safety Key Lab of Liaoning Province, National and Local Joint Engineering Research Center of Storage, Processing and Safety Control Technology for Fresh Agricultural and Aquatic Products, Jinzhou, Liaoning 121013, China

Tong Sun[a)]
College of Food Science and Project Engineering, Bohai University, Food Safety Key Lab of Liaoning Province, National and Local Joint Engineering Research Center of Storage, Processing and Safety Control Technology for Fresh Agricultural and Aquatic Products, Jinzhou, Liaoning 121013, China and School of Chemical Engineering, University of Birmingham, Edgbaston, Birmingham B15 2TT, United Kingdom

Zhibing Zhang and Zhenyu J. Zhang
School of Chemical Engineering, University of Birmingham, Edgbaston, Birmingham B15 2TT, United Kingdom

Jian-rong Li[a)]
College of Food Science and Project Engineering, Bohai University, Food Safety Key Lab of Liaoning Province, National and Local Joint Engineering Research Center of Storage, Processing and Safety Control Technology for Fresh Agricultural and Aquatic Products, Jinzhou, Liaoning 121013, China

(Received 23 December 2016; accepted 30 January 2017; published 9 February 2017)

Zinc oxide (ZnO) films were prepared on aluminum substrate by a hydrothermal method to investigate the effect of their surface characteristics, including morphology and hydrophobicity, on the corresponding antibiofilm performance. The surface characteristics of the prepared ZnO films were examined by a comprehensive range of methodologies, suggesting that films of distinctive surface morphologies were successfully formed. Subsequently, their antibiofilm activities, using *Shewanella putrefaciens* as a model bacterium, were assessed. Surface measurements confirmed that the ZnO films equipped with a nanoscopic needlelike surface feature are more hydrophobic than those possessing densely packed microflakes. The reduced number of live cells and presence of biofilm, confirmed by optical and electron microscopy results, suggest that the former films possess an excellent antibiofilm performance. It is believed that the engineered nanoscopic needle feature might penetrate the cell membrane when they are in contact, allowing the effective substance of ZnO antibacterial ingredients to diffuse into the embedded bacteria. Furthermore, such surface characteristics might perturb the integrity of the cell membrane causing the intracellular substance is leaked from the cells. As such, the combinatorial effects of nanoscopic feature resulted in an inhibited growth of *S. putrefaciens* biofilm on ZnO film. © *2017 American Vacuum Society*. [http://dx.doi.org/10.1116/1.4976003]

I. INTRODUCTION

Following the initial attachment to a surface or interface, bacterial cells are held together by the extracellular polymeric substance to form biofilm, which has significant implications in both industrial and personal applications.[1] One particular sector where biofilms cause serious engineering challenges is food industry because they could reduce heat transfer efficiency, increase fluid frictional resistance, and facilitate corrosion of the surfaces in contact.[2–4] Furthermore, during food processing and storage, biofilms can be found in corners, joints, and crevices, which significantly reduces the shelf life of commodity, increases the risk for food contamination, and leads to transmission of diseases.[5–7] Very often, biofilm of *Shewanella putrefaciens*, Gram-negative bacteria that can be isolated from fish, seawater, and sediment, is found on the surface of food processing equipment, pipelines, and raw materials, which causes huge economic loss in aquatic product industry.[8]

To prevent and suppress the formation of biofilm, embedding antibacterial metal ions as additive has been a strategy commonly implemented.[9,10] Among the few metal oxides that exhibit antimicrobial characteristics, zinc oxide (ZnO) has been used widely in food industry due to its excellent safety for human beings and animals and stability under high temperature and pressures usually associated with food processing.[11] Due to the small dimension and high surface-to-volume ratio, ZnO nanoparticles (ZnO-NPs) have been shown to be an effective food safety intervention approach to control microbial contamination. In a recent work, the antibacterial effect of ZnO nanoparticles on *Campylobacter jejuni* was examined for inhibition of cell growth, which showed that *C. jejuni* was very sensitive to the presence of ZnO nanoparticles.[12] Several mechanisms regarding the

[a)]Authors to whom correspondence should be addressed; electronic addresses: jzsuntong@sina.com; lijr6491@163.com

antibacterial abilities of ZnO-NPs have been proposed,[13,14] including dissolution of Zn^{2+} ions in aqueous suspension, generation of reactive oxygen species, and damage to the cell walls when in contact.

In addition to the chemical approach, functional surfaces with engineered features have been explored recently to enable antimicrobial performance. Singh and coworkers[15] reported that topography and roughness of nanostructured titanium surfaces are crucial to bacteria attachment and biofilm formation. The high surface roughness could inhibit protein adsorption, which in turn reduces bacterial adhesion and biofilm formation. Fisher *et al.*[16] reported that the sharp diamond nanocone features had bactericidal capabilities which surface possesses the more varying cone dimension, nonuniform array, and decreased density. It was also found that alumina surfaces with nanoscale topography can reduce attachment and biofilm formation of *Escherichia coli* and *Listeria* spp., and attributed such reduction to a synergic effect of electrostatic repulsion and surface effective free energy.[17] Even though the comprehensive antimicrobial mechanisms of super-hydrophobic surface remains unclear, it is commonly believed that such surface characteristics could result in reduced protein adsorption and entrapped air layer between bacterial cells and the surface.[18]

It is therefore desirable to integrate both of the approaches discussed above to develop a robust antimicrobial surface coating that combines ZnO material with functional surface features. For example, Mosnier *et al.*[19] reported that ZnO films, prepared by pulsed-laser deposition on soda lime glass substrates, could effectively inhibit the formation of *Staphylococcus epidermidis* biofilms by photocatalytic disinfection/inactivation, based on back-illumination with a ultraviolet A light source. A number of synthesis routes have been developed to prepare ZnO materials. These include electrochemical,[20] sol–gel,[21] hydrothermal,[14,22] and sonochemical[23] methods that result in ZnO nanoparticles or films of various features. Due to the mild reaction condition and uniform reaction system, hydrothermal method has been shown to enable preparation of uniform microstructure.

In the present work, ZnO films with various topographies were prepared on aluminum substrate followed by characterization of its crystal structure. To evaluate its antimicrobial performance, *S. putrefaciens* was used as representative bacteria to rationalize the antibiofilm mechanism. The research outcome could provide fundamental insight on whether ZnO film could be an effective approach as surface coating for equipment in food industry to inhibit biofilm formation.

II. MATERIALS AND METHODS

A. Materials

All chemicals were analytical grade and purchased from Tianjin Tianli Chemical Reagents, Ltd., and Tianjin Damao Chemical Reagent Factory (Tianjin, China). Deionized water (conductivity less than 0.5 mS/cm) and sterile water were used to prepare all the solutions. Lysogeny (LB) broth and LB nutrient agar were purchased from Qingdao Hope Bio-Technology Co., Ltd. (Tianjin, China). *S. putrefaciens* ATCC8071 was received from American Type Culture Collection.

B. Preparation and characterization of zinc oxide films on aluminum sheet

1. Preparation of zinc oxide films on aluminum sheet

Aluminum sheets with purity of 99.99% and thickness of 0.5 mm (Shengshida Metal Materials Co., Ltd., Shijiazhuang, China) were soaked in 1 mol/l sodium hydroxide solution for 2 s, rinsed thoroughly with deionized water, and finally dried in ambient. Solution of 0.05 mol/l zinc nitrate or 0.05 mol/l Zn^{2+} (mixture of 0.025 mol/l zinc acetate and 0.025 mol/l zinc chloride) was mixed with 0.05 mol/l hexamethylenetetramine solution with a molar ratio of 1:1, and transferred into a Teflon-lined stainless steel autoclave (ZhongKaiYa Stainless Steel Product Factory, Jiangsu, China). The aluminum sheets were then vertically positioned in the mixture, allowed to react at 95 °C for 12 h in a 100 ml reactor with a working volume of 75 ml (the filling ratio of 75%). After cooling to room temperature, the sheets were removed and rinsed thoroughly with deionized water, heated at 65 °C for 2 h in 2% Si-69 ethanol solution, and dried in vacuum. The ZnO films prepared by this method are named ZnO-1 and ZnO-2. Meanwhile, the precipitates were treated to get ZnO powders.

According to the volume ratio of triethanolamine (TEA) to 0.20 mol/l zinc acetate solution as 1:1 and 1:4, respectively, TEA was added into zinc acetate solution under constant stirring. The mixture was then transferred to a Teflon-lined stainless steel autoclave at the filling ratio of 75%, and the aluminum sheet was vertically positioned. After reaction at 160 °C for 2 h and cooling to room temperature, the sheets were rinsed with deionized water, heated at 65 °C for 2 h in 2%Si-69 ethanol solution, and vacuum dried to obtain samples ZnO-3 and ZnO-4. At the same time, the precipitates were treated to gain ZnO powders.

2. Characterization of zinc oxide films on aluminum surface

To characterize the crystalline properties of the ZnO powders that were prepared simultaneously with the ZnO films, x-ray diffraction (XRD) measurements of ZnO powders were performed (Rigaku Ultima IV, Rigaku, Japan) using Cu Kα radiation ($\lambda = 0.15405$ nm), scanned in 2θ range from 10° to 70° with 6°/min scanning speed at a step of 0.02°. FT-IR spectra of the samples removed from the zinc oxide films were acquired using a Scimitar 2000 Near FT-IR Spectrometer (Agilent) from 4000 to 400 cm^{-1} by KBr pellets method. Scanning electron microscopy (SEM) was performed to analyze the surface topography of ZnO films with S-4800 SEM (Hitachi, Japan) at 3 kV. Transmission electron microscopy (Jem-2100F, Electronic Co., Ltd., Japan) and selected-area electron diffraction (SAED) techniques were used to characterize the morphological properties of ZnO films. ZnO film samples removed from aluminum

sheets were dispersed in ethanol via sonication, then deposited on a carbon coated copper grid that was dried at room temperature. The prepared copper grid was fixed in a sample holder and analyzed at 200 kV in the TEM. The hydrophilic properties of ZnO films were measured based on the water contact angles method using an OCA15EC type contact angle tester (Dataphsics, Germany). The surface roughness of ZnO films was measured by atomic force microscopy (XE-70, Park Systems, Republic of Korea).

C. Cultivation and characterization of *S. putrefaciens* biofilms

1. *Cultivation of* S. putrefaciens *biofilms*

The mixed bacterial suspension was prepared according to a volume ratio of bacterial suspension (cell density of 1×10^7 cfu/ml) to culture medium 1:200. The bacterial suspension (1 ml) was then added into a centrifuge tube as culture device. The aluminum sheet with ZnO film (0.5×0.5 cm) was placed in the centrifuge tube and cultivated at 28 °C. Three parallel experiments were performed, and the results are expressed as "average value ± standard deviation."

2. *Adhesion analysis of* S. putrefaciens *biofilms*

After cultivating for a certain period, the aluminum sheet with ZnO films was removed and placed in a sterile centrifugal tube, rinsed with sterile water to remove the planktonic bacteria. Then, 1 ml of 0.2% crystal violet solution was added to stain the aluminum sheet for 5 min, and excess dye was removed by washing twice with sterile water. The sheet was destained with 0.2 ml of 95% ethanol (v/v) for 5 min, and the optical density was measured at 595 nm (OD_{595}) with a VICTOR™ X3 microplate reader (Perkin Elmer), which indicates the total amount of the biofilm.

3. *Growth curve of* S. putrefaciens *in the biofilms*

After cultivating for a certain time, the aluminum sheet with ZnO films was removed and washed with sterile phosphate buffer solution for three times to eliminate planktonic bacteria. The sheet was placed in 10 ml phosphate buffer solution and ultrasonically treated at 25 °C for 10 min. Plate counting method was used to measure the growth curve of biofilms.

4. *SEM and CLSM analysis of* S. putrefaciens *biofilms*

Biofilms formed on the ZnO films were fixed by 2.5% (v/v) glutaraldehyde at 4 °C for 4 h, then dehydrated using ethanol solutions of 50%, 70%, 80%, 90% (*v*/*v*) for 10 min each and 100% for 15 min. After vacuum drying and gold sputtering, the samples were imaged by a scanning electron microscope at 2 kV (S-4800, Hitachi, Japan). Confocal laser scanning microscopy (CLSM) (TCS-SP5 II, Leica Instrument Co., Germany) was used to observe the proportions of live and dead cells in the biofilms.[24] Two milligram of acridine orange (AO, Sigma-Aldrich) was dissolved in 1 ml phosphate buffer saline (PBS, *p*H = 7.4) to get 0.2 wt. % AO solution, and 5 mg propidium iodide (PI, Sigma) was dissolved in 250 μl PBS to get 2.0 wt. % PI solution. After being thoroughly washed with PBS for three times, the ZnO film with biofilm was exposed to the mixed solution of 0.01% AO and 0.1% PI, and then was stained in dark for 15 min. After washing with PBS for three times and the excess moisture water absorbed, the samples were infused in 50 μl antifluorescence quenching sealing agents (Biosharp BL701A, China) and were stored at 4° in dark. The samples were then imaged by confocal laser scanning microscopy with laser light of 488 nm as excitation light source of green and 543 nm as that of red.

III. RESULTS AND DISCUSSION

A. Characterization of the ZnO films

Four different ZnO film samples were prepared on alumina substrate in the present work. Samples ZnO-1 and ZnO-2 were prepared at 95 °C for 12 h with molar ratio of Zn^{2+} to hexamethylenetetramine being 1:1 (Zn^{2+} is zinc nitrate and a mixture of zinc acetate and zinc chloride, respectively). Samples ZnO-3 and ZnO-4 were produced at 160 °C for 2 h in a mixture of TEA and 10 mmol/l $Zn(CH_3COOH)_2$ (volume ratio 1:1 and 1:4, respectively).

1. *XRD and FT-IR characterization of the ZnO films*

It has been reported previously that the antibiofilm properties of zinc oxide could be influenced by its crystal form, e.g., Khan *et al*. found that the shape of NPs may affect biofilm formation,[25] while Dutta *et al*. concluded that unusual crystal morphologies may affect antimicrobial effects.[26] To characterize the crystal form of the prepared ZnO films, XRD measurements of the ZnO powders synthesized under the same reaction conditions were preformed, and FT-IR spectra were obtained to verify the combined state of zinc oxide and substrate.

XRD results presented in Fig. 1(a) show that there are strong diffraction peaks at 31.7°, 34.4°, 36.2°, 47.5°, 56.6°, 62.8°, 66.3°, 67.9°, and 69.1° of 2θ which correspond to (100), (002), (101), (102), (110), (103), (200), (112), and (201) crystal planes of zinc oxide crystal, respectively, confirming that the samples are hexagonal phase of ZnO (PDF#35-1451). The high intensity of the diffraction peaks of ZnO-1 and ZnO-2 suggests that the samples have high crystallinity and large crystal particles. For sample ZnO-3, the diffraction peaks at 36.3°, 39.0°, 43.2°, and 54.3° of 2θ correspond to (002), (100), (101), and (102) crystal planes of zinc (PDF#65-5973). This may be that a part of zinc oxide is reduced to zinc by aluminum. Meanwhile, the wide diffraction peaks suggest that the crystallinity of ZnO-3 is low, and the crystal particles are small. In addition, no peak of alumina appears in the results, which may result from that the test powders contain a small quantity of substrate composition and the intensity of unit mass alumina is weak. The XRD spectrum of ZnO-4 was not obtained due to very low yield of the powder, but its crystal structure could be deduced to be similar as that of ZnO-3 because of their same reaction condition.

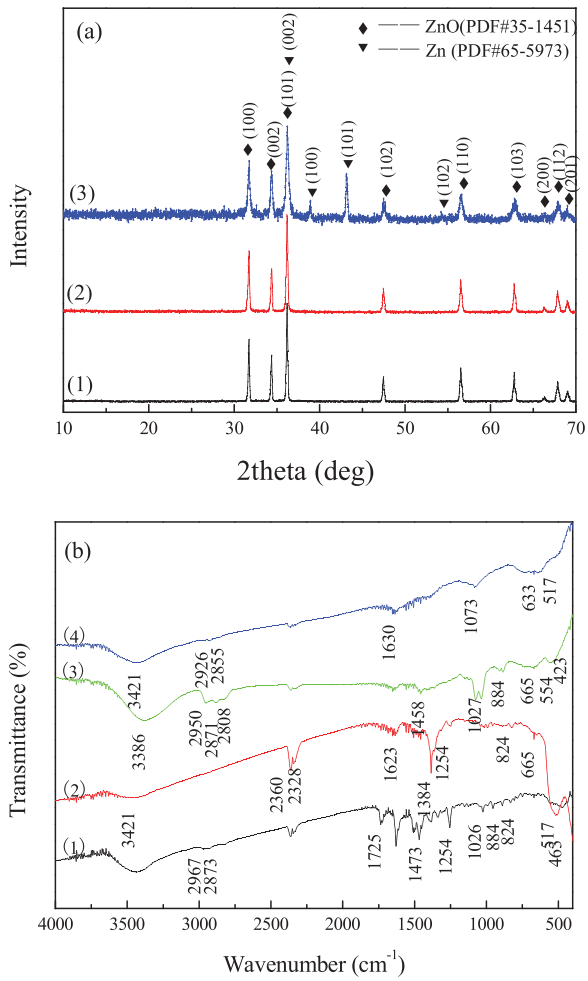

FIG. 1. XRD spectra (a) and FT-IR spectra (b) of the ZnO film samples used in the present work: (1) ZnO-1; (2) ZnO-2; (3) ZnO-3; and (4) ZnO-4.

FT-IR spectra of the samples are shown in Fig. 1(b). Peaks observed at around 3500–3300 cm^{-1} and at 1630–1623 cm^{-1} are due to the stretching vibration and the bending vibration of –OH group, respectively, which indicates the presence of absorbed water and pore water in all samples.[27] The peaks at 2360 and 2328 cm^{-1} are due to the presence of carbon dioxide in the ambient. In addition, the peaks at 884 and 824 cm^{-1} are attributed to the stretching vibration of Zn–OH–Zn and Zn–OH, and the peaks at 665–633 cm^{-1} are attributed to vibration of AlO_6.[28] The peaks at 554–517 cm^{-1} are generated by vibration of Zn–O, and the peaks at 463–423 cm^{-1} are assigned to vibration of Al–O.[29]

Furthermore, the peaks at 2967 and 2873 cm^{-1} are attributed to asymmetric and symmetric stretching vibration of $–CH_3$ group, respectively, while the peak at 1473 cm^{-1} is due to asymmetric bending vibration of $–CH_3$ group. Finally, the peak at 1725 cm^{-1} is attributed to stretching vibration of –C=O, and the peaks at 1254 and 1026 cm^{-1} are attributed to asymmetric stretching vibration of –O–C–C and stretching vibration of –O–C.[30] The results confirm the presence of $–CH_3$, –C=O, and –O–C functional groups on the sample surface, which could be attributed to the adsorbed formaldehyde as the result of decomposition of hexamethylenetetramine during the hydrothermal process.

Unlike sample ZnO-1, the above discussed peaks associated with formaldehyde are reduced significantly in sample ZnO-2, suggesting that hexamethylenetetramine did not decompose in the preparation of ZnO-2. It is probable that the acidity of the hydrothermal system increased when preparing ZnO-1 sample, which caused hexamethylenetetramine to decompose. As shown in Fig. 1(b), the peaks at 2950, 2871, and 1458 cm^{-1} observed on sample ZnO-3 are due to $–CH_3$, while the peaks at 2926 and 2855 cm^{-1} acquired on sample ZnO-4 are due to asymmetric and symmetric stretching vibration of $–CH_2$, respectively. Furthermore, the peak at 1073 cm^{-1} is due to stretching vibration of –C–O of primary alcohol. In the hydrothermal system of ZnO-3, aluminum sheets were corroded by high concentration of TEA, as such, $–CH_3$ were formed. However, in the hydrothermal system of ZnO-4, low concentration of TEA caused little corrosion to aluminum, so that there was no $–CH_3$ presence in the FTIR spectrum.

Overall, both XRD and FT-IR results confirm that the underlying aluminum sheet was involved in the hydrothermal synthesis of ZnO samples, and that the ZnO films were successfully deposited on the aluminum substrate by chemical bonds in all samples.

2. SEM analysis of the ZnO films

It has been reported that both surface topography and roughness are crucial to bacterial attachment and biofilm formation, and that nanoscopic surface features can strongly influence the adhesion of biofilm on solid substrates.[15] Following the surface chemical characterization, surface morphologies of the ZnO films were examined by SEM. Figure 2(a) shows that flakes with more than 100 nm thickness and 2 μm length are randomly packed in sample ZnO-1, whereas sheets of reduced thickness (~40 nm) and broad diameter (~4 μm) were assembled into a more organized configuration [Fig. 2(b)]. It is possible that due to the decomposition of hexamethylenetetramine in the hydrothermal preparation process of sample ZnO-1, there was a lack of coordination and guiding function associated with hexamethylenetetramine,[31] which resulted the variation in morphology between samples ZnO-1 and ZnO-2.

Figures 2(c) and 2(d) show that ZnO films consist of features with reduced size and drastically changed geometry. Needlelike features, with length about 2 μm assembled in an organized microstructure, were observed on sample ZnO-3. However, such microstructure is no longer present on sample ZnO-4, and the nanofeatures are distributed evenly across the surface. Moreover, it has been confirmed in the feature that TEA could guide the formation of ZnO crystals and the presence of such surface, leading to formation of sharp nanoneedles.[32,33] However, in the hydrothermal process of ZnO-4, less TEA was available to guide the zinc oxide crystal, resulting in a different pattern from ZnO-3.

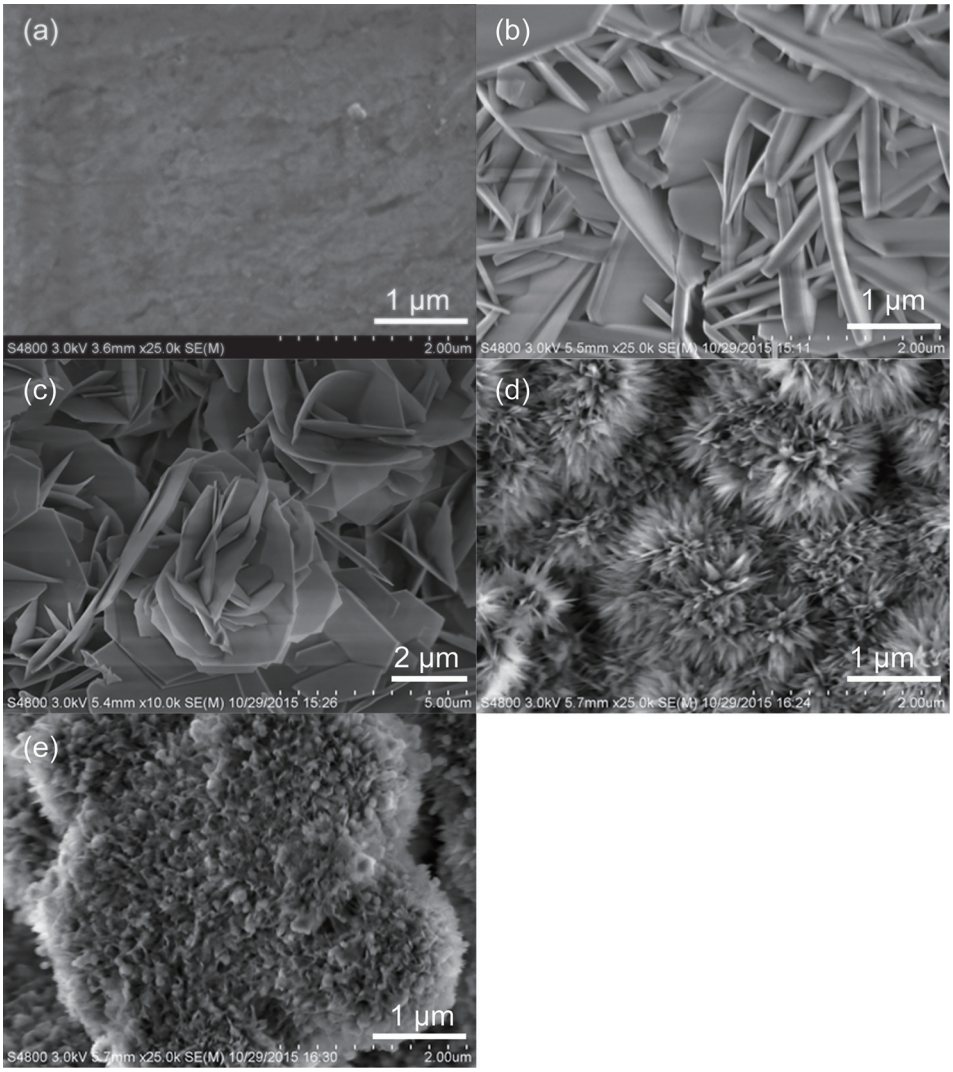

FIG. 2. SEM images of ZnO films (scale bars are included in the corresponding image): (a) ZnO-1; (b) ZnO-2; (c) ZnO-3; and (d) ZnO-4.

3. TEM and SAED of the ZnO films

Following SEM measurements, TEM and SAED were performed on ZnO films to investigate their detailed structure. Figure 3(a) shows that microflakes of ZnO-1 are uniformly arranged, containing ZnO nanoparticles less than 5 nm, while the nanosheets of ZnO-2 consist of nanoparticles of 20–30 nm [Fig. 3(b)]. However, as shown in Figs. 3(c) and 3(d), ZnO-3 and ZnO-4 are in the form of nanoneedles without microscopic structure, illustrating that the crystal particles are small, which is consistent with the XRD results. SAED pattern of ZnO-2 shows (100), (101), (102), (110), and (103) crystal planes of zinc oxide crystal [Fig. 3(e)]. SAED pattern of ZnO-3 shows (101), (102), and (201) crystal planes of zinc oxide crystal and (002) and (100) crystal planes of zinc crystal simultaneously. The results are consistent with XRD results.

4. Contact angles of the ZnO films

It was reported that *L. monocytogenes* adhered greater to hydrophilic surfaces than to hydrophobic ones under the same growth condition (20 °C for 24 h)—93.8% and 81.3% biofilms were formed on hydrophilic surfaces (stainless steel and glass, respectively), with just 6.2% on hydrophobic surface (polystyrene).[34] Türetgen[35] reported that hydrophobic nanosilica coating could substantially reduce (up to four magnitude) biofilm formation on fill material in a cooling tower after examining coupons that were exposed to the bacteria. Schaer *et al.*[36] found that hydrophobic coatings can inhibit biofilms formation—covering surfaces with hydrophobic coatings could significantly reduce bacterial attachment and adhesion. To elucidate the effect of hydrophobicity of the ZnO films on the formation of biofilms, water contact angles on their surface were measured to examine their surface energy with results presented in Table I.

The results show that both ZnO-1 and ZnO-2 samples are relatively hydrophilic, with ZnO-2 being more hydrophilic. However, ZnO-3 and ZnO-4 samples exihibit much increased contact angles, indicating that they both are hydrophobic. Meanwhile, the surface roughness of both ZnO-1 and ZnO-2 samples are smaller than that of ZnO-3 and ZnO-4.[41] The contact angle results can be rationalized by their

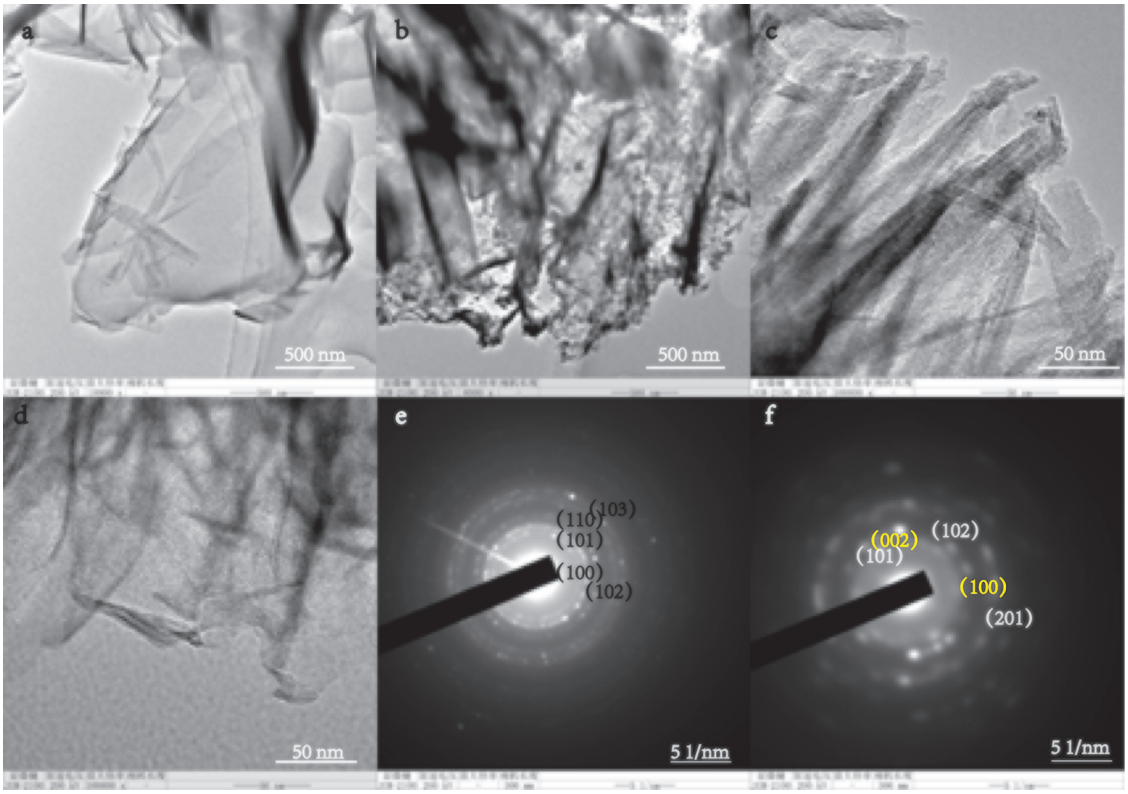

FIG. 3. TEM images and SAED patterns of the ZnO films: (a) TEM images of ZnO-1; (b) ZnO-2; (c) ZnO-3; (d) ZnO-4; (e) SAED patterns of ZnO-2; and (f) ZnO-3.

surface morphology and surface roughness that was examined by the electron microscope. Flakelike features of micron size were observed in the first two samples, whereas the size of the features is within nanometer range for samples ZnO-3 and ZnO-4. It is believed that the needlelike features with microstructure on the surfaces created the "Lotus Effect" resulting in their increased contact angles.[37] Even though the size of the needlelike features on samples ZnO-3 and ZnO-4 was similar, these features are distributed more evenly on ZnO-4, which effectively reduce surface roughness and contact angle.[38,39]

B. Adhesion and growth curve analysis of *S. putrefaciens* biofilm

It is generally accepted that the biofilm formation can be described by five stages: (1) initial reversible attachment of bacteria, (2) transition from reversible to irreversible attachment, (3) early development of biofilm structure, (4) development of microcolonies into a mature biofilm, (5) dispersion of cells from the biofilm and return to the planktonic state.[5] To test the antimicrobial performance of the ZnO film samples, the total amount of biofilm (the optical density, OD_{595}), and viable count of *S. putrefaciens* were measured as a function of time, as shown in Fig. 4. Figure 4(a) shows that OD_{595} increases rapidly in the first 2 h, suggesting that the attachment of bacteria transforms to irreversible attachment from initial reversible attachment. From 2 to 24 h of growth time, the OD_{595} increases slowly for all samples, which could be attributed to the early development and formation of biofilm. After 24 h, the OD_{595} increases rapidly again which is due to the maturation of the biofilm. And after 36 h, the adhesion properties reduce sharply, indicating that the cells might enter a death phase. At all stages, it appears there is no significantly consistent difference in the optical density between the four samples due to the large error bars. Consequently, the influence of nanoscopic structure and hydrophobicity on the total amount of biofilm could not be reliably distinguished between the samples.

Figure 4(b) presents the total number of viable bacteria on all ZnO film samples as a function of time. The overall growth curves show that the amount of cells on ZnO-3 increased slowly, while there is no significant difference between the other three samples up to 24 h. The result clearly demonstrates that ZnO-3 sample has the best antimicrobial ability as opposed to the other three samples during the adhesion and early development stage of biofilm. It is likely that the nanoscopic needlelike feature could penetrate through the cell membrane when they are in contact with the

TABLE I. Surface roughness and contact angle of the ZnO films.

Sample	Surface roughness (nm)	Contact angle (deg)
Al	18.8	
ZnO-1	56.8	83.5 ± 0.2
ZnO-2	83.5	69.4 ± 0.2
ZnO-3	483.5	129.7 ± 0.1
ZnO-4	229.0	113.3 ± 0.3

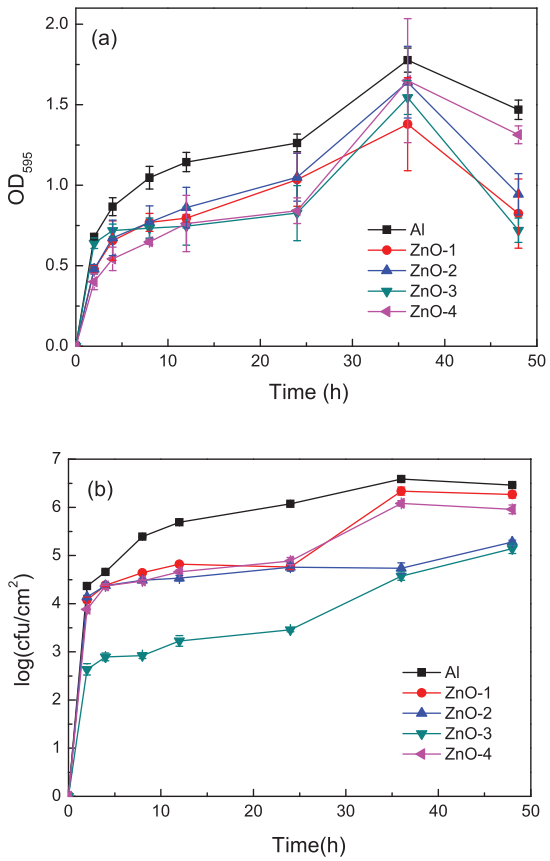

FIG. 4. Total amount (a) and viable count (b) of the biofilms on the zinc oxide films. [The error bars are too small to be visible in Fig. 4(b).]

bacteria, which not only allows the intracellular substance to leak from cells, but also generates the pathway for the effective antibacterial substance of ZnO to diffuse into the bacteria with biofilm.[40] Such combinatorial effect of chemical and physical intervention as a consequence of nanoscopic needlelike feature could damage the integrity of the cell membrane, hence inhibit growth of bacteria in the biofilm.[19]

It is also worth noting that at the mature biofilm stage (24–36 h), the total number of bacteria of ZnO-2 grows more slowly, the other two samples continued to grow, and the total number of bacteria of ZnO-3 grow sharply, illustrating that the ZnO-2 film has strong antimicrobial effect at this stage. This may be due to the larger specific surface area of the thin sheet ZnO in ZnO-2, and the effective antimicrobial substances can continue to penetrate into the biofilm bacteria. However, the extracellular polymeric substances (EPS) of biofilm attached to the surface of ZnO-3 prevents the antimicrobial components of ZnO to lixiviate into the embedded bacteria, leading to a significant increase in viable cell number at this stage. During the death period (after 36 h), it was noted that the number of cells for ZnO-2 and ZnO-3 increased continuously, while the growth on the other two samples is negligible. It is likely that the attached polysaccharide of biofilm adheres tightly on the pinpoint of nanoneedle in ZnO-2 and ZnO-3 samples, so that the antibacterial properties of ZnO are inhibited, and the bacteria in the biofilm continued to grow. For the other two samples, the nutritional composition of biofilm decreases due to the decrease of adhered EPS, so that the live bacteria detach from the biofilm.

C. Morphology of *S. putrefaciens* biofilms

Biofilm formed on the ZnO films was collected at various stages of growth and imaged by the scanning electron microscopy, and the proportions of live and dead cells in the biofilms were observed by confocal laser scanning microscopy. The images presented in Fig. 5 show the morphologies of biofilm on two representative ZnO film samples (ZnO-2 and ZnO-3), and Fig. 6 shows the proportions of live (green) and dead (red) cells on the same samples. At 2 h, the presence of organic residue (EPS) and less live bacteria on ZnO film samples confirms the stage of initial reversible and irreversible attachment of bacteria. At 12 h, EPS and some bacteria were observed on the ZnO samples, which indicates the transition from dynamic attachment to the development biofilm structure. It is noticeable that the number of bacteria on ZnO-2 is more than ZnO-3 film, which is consistent with the adhesion rate and the number

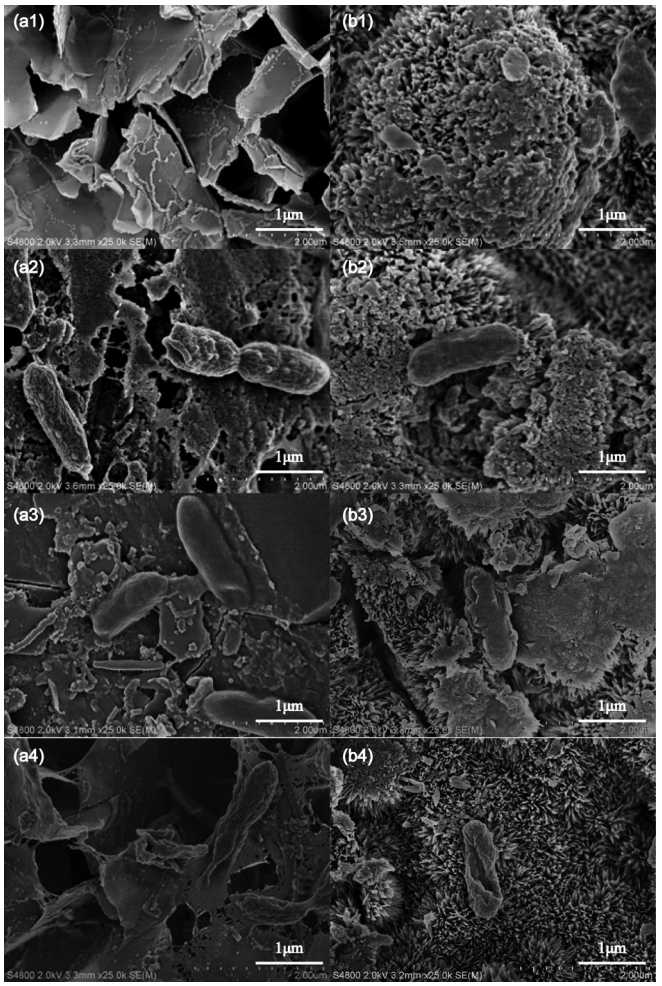

FIG. 5. SEM images of biofilms formed on two representative ZnO films prepared at different growth stages: (a) ZnO-2; (b) ZnO-3 (1) 2 h; (2)12 h; (3) 24 h; and (4) 48 h.

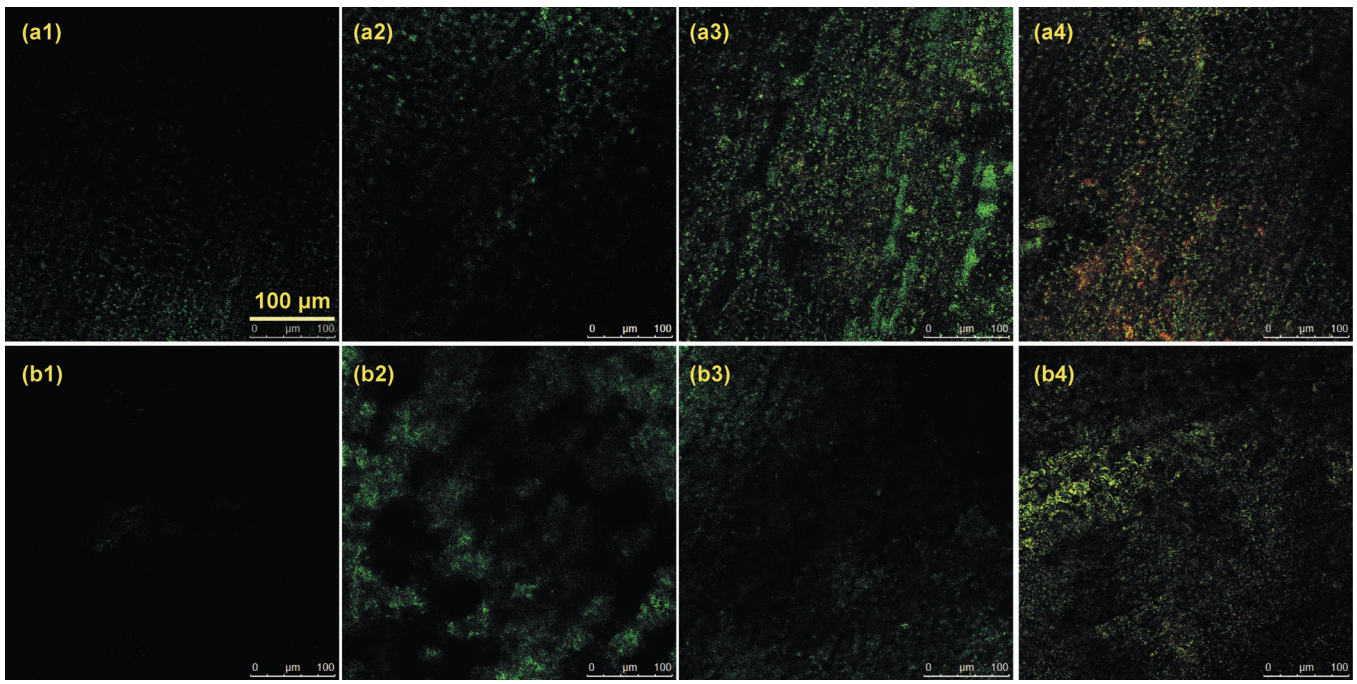

FIG. 6. CLSM images of biofilms formed on two representative ZnO films prepared at different growth stages: (a) ZnO-2; (b) ZnO-3 (1) 2 h; (2)12 h; (3) 24 h; and (4) 48 h.

of live bacteria results in Fig. 4. Such variation confirms that the enhanced hydrophobicity and the reduced size of surface feature could effectively impede biofilm growth. Samples collected at 24 h present a thick polysacharide film, and less bacteria can be seen on ZnO-3. It is probably due to the antibacterial substance of ZnO permeates into the bacteria within biofilm, and consequently disturbs the integrity of the cell membrane.

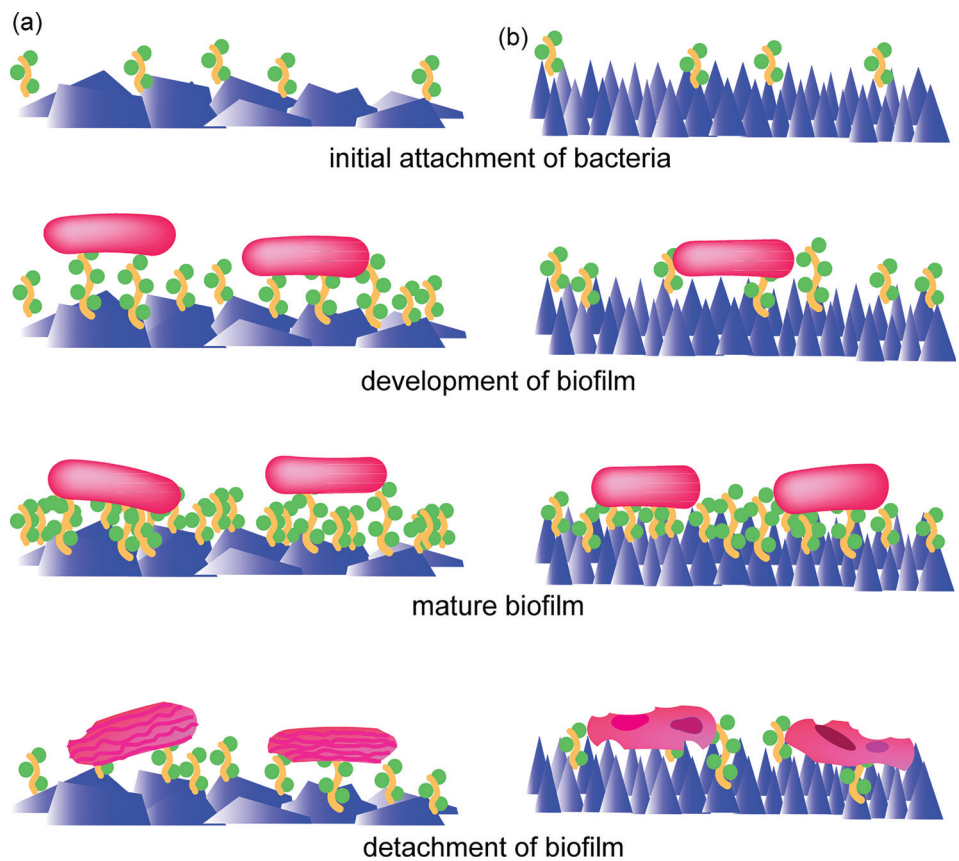

FIG. 7. Schematic drawing of biofilms formation: (a) nanoflakes features of ZnO film; (b) nano-needle-like features of ZnO film.

Damaged cells were observed on both ZnO samples during death phase at 48 h, and more dead bacteria are presented. As shown in Fig. 5(a4), the cell membrane is clotted, even though the cells are intact on ZnO-2 sample. On the contrary, it was observed on ZnO-3 that the cell membrane of damaged cells is fractured, and there was leaked intracellular substance on the ZnO film. The distinctive comparison confirms our rational that the combinatorial effect of nanoscopic needle-feature has a great impact on the growth of biofilm.

Based on above discussion, the formation mechanism of the biofilms on the ZnO films might be described by the schematic diagrams in Fig. 7. At the initial attachment stage, organic residue (EPS) presents on the ZnO film, then more organic residue and embedded bacteria are the ZnO films at the stage of biofilm development. At the biofilm maturation stage, polysacharide films on the ZnO surface thicken unceasingly, and the embedded bacteria are well grown. However, at the death phase of the biofilm, the polysacharide films fall away from ZnO films, and the bacterial cells are damaged. The surface structure of ZnO film only affected the last stage of biofilm development. At the biofilm death phase, the intact cells with clotted membrane are present on the ZnO films with microflakes, but the fractured cells with clotted membrane appear on the ZnO films with nanoneedles structure. It may be the combinatorial effect of nanoscopic needle-feature and antibacterial properties of ZnO that were responsible for the lowest viable cell number in ZnO-3 at any given time among the four samples investigated.

IV. CONCLUSIONS

In the present work, various ZnO films were prepared on aluminum substrates using facile hydrothermal method under different preparation conditions. Their surface characteristics were investigated by both physical and chemical methods to examine their morphology and hydrophobicity. It was found that the ZnO films equipped with nanoscopic needlelike feature assembled in organized fashion exhibit great hydrophobicity. However, the effect of nanoscopic structure and hydrophobicity of ZnO film on the total amount of biofilm could not be reliably demonstrated. Nevertheless, it has been found that the ZnO film with nanoscopic needlelike feature (ZnO-3) was most effective in inhibiting the growth of viable cells at any given time, which was attributed that the nanoscopic needle structure could penetrate the cell membrane and ZnO have an antimicrobial effect when in contact, which kills the cells attached on the surface. The combinatorial approach that integrates both functional surface feature and effective antimicrobial metal oxide could have great potential in prevention of biofilm growth with a wide range of applications.

ACKNOWLEDGMENTS

This study was supported by The National Natural Science Foundation of China (No. 31371858), the National 12th Five-Year Science and Technology Supporting Plan in China (No. 2015BAD17B03), Food Safety Key Laboratory of Liaoning Province, and Engineering and Technology Research Center of Food Preservation, Processing, and Safety Control of Liaoning Province.

[1]T. R. Garrett, M. Bhakoo, and Z. Zhang, Prog. Nat. Sci. **18**, 1049 (2008).
[2]S. Srey, I. K. Jahid, and S.-D. Ha, Food Control **31**, 572 (2013).
[3]C. Ganesh Kumar and S. K. Anand, Int. J. Food Microbiol. **42**, 9 (1998).
[4]X. Shi and X. Zhu, Trends Food Sci. Technol. **20**, 407 (2009).
[5]R. Van Houdt and C. W. Michiels, Res. Microbiol. **156**, 626 (2005).
[6]M. Hjelm, L. R. Hilbert, P. Møller, and L. Gram, J. Appl. Microbiol. **92**, 903 (2002).
[7]W. M. Dunne, Clin. Microbiol. Rev. **15**, 155 (2002).
[8]R. Van Houdt and C. W. Michiels, J. Appl. Microbiol. **109**, 1117 (2010).
[9]A. Asatekin, A. Menniti, S. Kang, M. Elimelech, E. Morgenroth, and A. M. Mayes, J. Membr. Sci. **285**, 81 (2006).
[10]A. Akthakul, R. F. Salinaro, and A. M. Mayes, Macromolecules **37**, 7663 (2004).
[11]J. Pasquet, Y. Chevalier, J. Pelletier, E. Couval, D. Bouvier, and M.-A. Bolzinger, Colloids Surf., A **457**, 263 (2014).
[12]Y. Xie, Y. He, P. L. Irwin, T. Jin, and X. Shi, Appl. Environ. Microbiol. **77**, 2325 (2011).
[13]L. Zhang, Y. Jiang, Y. Ding, N. Daskalakis, L. Jeuken, M. Povey, A. J. O'Neill, and D. W. York, J. Nanopart. Res. **12**, 1625 (2010).
[14]N. Talebian, S. M. Amininezhad, and M. Doudi, J. Photochem. Photobiol., B **120**, 66 (2013).
[15]A. Vikram Singh *et al.*, Plos One **6**, e25029 (2011).
[16]L. E. Fisher, Y. Yang, M. F. Yuen, W. Zhang, A. H. Nobbs, and B. Su, Biointerphases **11**, 011014 (2016).
[17]G. Feng, Y. Cheng, S. Y. Wang, L. C. Hsu, Y. Feliz, D. A. Borca-Tasciuc, R. W. Worobo, and C. I. Moraru, Biofouling **30**, 1253 (2014).
[18]X. Zhang, L. Wang, and E. Levänen, RSC Adv. **3**, 12003 (2013).
[19]J.-P. Mosnier, R. J. O'Haire, E. McGlynn, M. O. Henry, S. J. McDonnell, M. A. Boyle, and K. G. McGuigan, Sci. Technol. Adv. Mater. **10**, 045003 (2009).
[20]T.-J. Whang, M.-T. Hsieh, J.-M. Tsai, and S.-J. Lee, Appl. Surf. Sci. **257**, 9539 (2011).
[21]L. Cui, G.-G. Wang, H.-Y. Zhang, R. Sun, X.-P. Kuang, and J.-C. Han, Ceram. Int. **39**, 3261 (2013).
[22]J.-J. Dong, C.-Y. Zhen, H.-Y. Hao, J. Xing, Z.-L. Zhang, Z.-Y. Zheng, and X.-W. Zhang, Nanoscale Res. Lett. **8**, 1 (2013).
[23]A.-Q. Zhang, L. Zhang, L. Sui, D.-J. Qian, and M. Chen, Cryst. Res. Technol. **48**, 947 (2013).
[24]E. P. Ivanova *et al.*, Nat. Commun. **4**, 2838 (2013).
[25]S. Tabrez Khan, M. Ahamed, A. Al-Khedhairy, and J. Musarrat, Mater. Lett. **97**, 67 (2013).
[26]R. K. Dutta, B. P. Nenavathu, M. K. Gangishetty, and A. V. Reddy, Colloids Surf., B **94**, 143 (2012).
[27]T. Sun, C.-L. Wu, H. Hao, Y. Dai, and J.-R. Li, Food Hydrocolloids **54**, 130 (2016).
[28]S.-B. Mao, D.-Q. Li, F.-Z. Zhang, D. Evans, and X. Duan, Chin. J. Inorg. Chem. **20**, 596 (2004).
[29]T. Sun, H. Hao, W. T. Hao, S. M. Yi, X. P. Li, and J. R. Li, Nanoscale Res. Lett. **9**, 98 (2014).
[30]S.-P. Wang, *Principle and Technology of Modern Instrument Analysis* (Science, Beijing, 2016).
[31]H. Lu, S. Wang, L. Zhao, J. Li, B. Dong, and Z. Xu, J. Mater. Chem. **21**, 4228 (2011).
[32]G.-H. Shen and F. C.-N. Hong, Thin Solid Films **570**, 363 (2014).
[33]A. K. Zak, R. Razali, W. H. Majid, and M. Darroudi, Int. J. Nanomed. **6**, 1399 (2011).
[34]E. C. R. Bonsaglia, N. C. C. Silva, A. Fernades Júnior, J. P. Araújo Júnior, M. H. Tsunemi, and V. L. M. Rall, Food Control **35**, 386 (2014).
[35]I. Turetgen, Water SA **41**, 295 (2015).
[36]T. P. Schaer, S. Stewart, B. B. Hsu, and A. M. Klibanov, Biomaterials **33**, 1245 (2012).
[37]V. Baeyer and H. Christian, Sciences **40**, 12 (2000).
[38]D. Quéré, Physica A **313**, 32 (2002).
[39]A. Marmur, Biofouling **22**, 107 (2006).
[40]Y. Jiang, L. Zhang, D. Wen, and Y. Ding, Mater. Sci. Eng., C **69**, 1361 (2016).
[41]See supplementary material at http://dx.doi.org/10.1116/1.4976003 for the results of AFM of the samples. It is related to the roughness of the samples.